scientific reports

Check for updates

OPEN

Efficient photocatalytic degradation of petroleum oil spills in seawater using a metal-organic framework (MOF)

M. S. Showman[1]✉, Asmaa M. Abd El-Aziz[1] & Rana Yahya[2]

Photocatalysis is a green approach that has appeared to be a viable option for the degradation of a variety of organic contaminants. This work outlines the process of preparing the titanium-based metal-organic framework (MIL-125) photocatalysts using a simple solvothermal method. Structural, morphological, and optical analysis of samples (MT18 and MT48) was carried out by XRD, FT-IR, Raman, SEM, TGA, BET, and UV–Vis. Results indicated that the sample prepared at 150 °C and reaction time of 48 h (MT48) has a low crystal size of 7 nm with an optical band gap of 3.2 eV and a surface area of 301 $m^2 g^{-1}$. Under UV–visible light irradiation, the as-prepared MOFs proved to upgrade photocatalytic activity in degrading crude oil spills in saltwater. Effects of catalyst dosage and exposure time on the degradation of an oil spill in seawater were studied and analyzed using UV–Vis spectrophotometry and gas chromatography (GC–MS) which emphasized that the use of 250 ppm of MT48 photocatalyst under UV–Vis irradiation can degrade about 99% of oil spills in water after 2 h of exposure. The study's data revealed that MIL-125 could be used to photocatalyzed the cleanup of crude oil spills.

Marine oil spills typically relate to human activities that result in the release of liquid petroleum hydrocarbons into the ocean or coastal areas. They entail the release of crude oil from ships, offshore platforms, drilling rigs, and wells. Spills of crude oil can cause enormous economic losses and damage to ecological systems, public health, and communities[1]. Crude oil can be used not only as fuel and gasoline but also as a raw material for industrial products, such as fertilizers, pesticides, and plastics[2]. Dissolution, emulsification, absorption, mixing, evaporation, biodegradation, photodegradation, and chemical reactions all contribute to the degradation and dispersion of aquatic discharged oil[3].

Photocatalytic oxidation is a method of converting oil into carbon dioxide, water, and salts using light as a driving energy source. Catalyzed advanced oxidation processes (AOPs) in aqueous media generate hydroxyl radicals, which are highly reactive with nonselective chemicals and have a high oxidation potential ($E_o = 2.8$ V) to destroy petroleum hydrocarbon molecules, allowing them to react with a wide range of oil pollutants[4].

Metal-organic frameworks (MOFs) have attracted the interest of researchers because to their unusually large specific surface areas and open, interconnected microporous architectures, a high proportion of transition metals, and the capacity to be customized and modified after synthesis, and their ability to exhibit semiconductor-like behavior[5,6]. To date, more than 20,000 MOFs have been designed and synthesized. Most of those MOFs' applications, however, are hampered by their unstable nature. Aiming at realizing a more stable MOF, extensive efforts have been made by researchers around the world. Among the various semiconductors, TiO_2 is the first example used for photocatalytic hydrogen production due to its light sensitive Ti ions. Superior to TiO_2, MIL-125 not only possess Ti-oxo clusters or Ti-oxo chains/sheets, but also have light harvested ligands, endowing them with promising photocatalytic activity. The adjustable structures of MIL-125, in particular, allow them to efficiently utilise solar light beyond the ultraviolet region (which accounts for only 4% of the total)[7–9]. The stability properties of MOFs mainly contain four factors, such as chemical stability, photostability, mechanical stability, and thermal stability[10,11].

In the photocatalysis mechanism, photogenerated electrons and holes are separated and used in the same way as they are in traditional semiconductors[12,13]. When the photon energy is greater than or equal to the MIL-125

[1]Fabrication Technology Research Department, Advanced Technology and New Materials Research Institute, City of Scientific Research and Technological Applications, Alexandria, Egypt. [2]Department of Chemistry, College of Science, University of Jeddah, Jeddah, Saudi Arabia. ✉email: marwashowman@yahoo.com

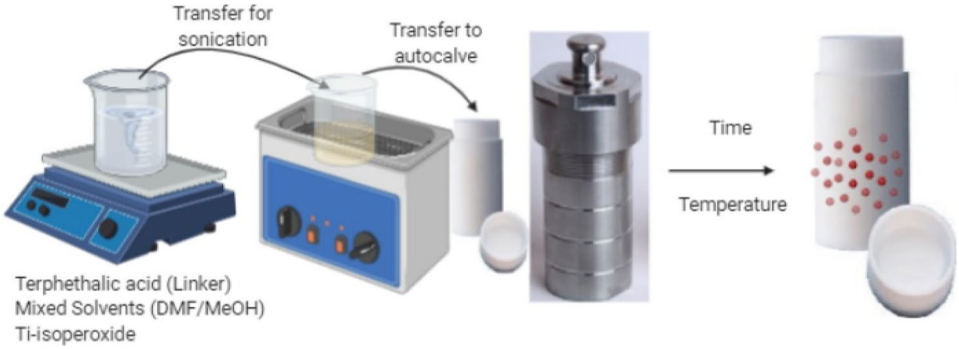

Figure 1. Detailed preparation methods of the solvothermal preparation of Ti-MOFs.

bandgap, the MIL-125 can be stimulated by light to generate photo-generated electrons and holes[14,15]. Electrons are stimulated from the highest occupied molecular orbital (HOMO) of the organic linker to its lowest unoccupied molecular orbital (LUMO). The photoexcited electrons are then passed to the MOF nodes via a linker-cluster charge transfer mechanism (LCCT), which activates the metal nodes and allows them to participate in the photooxidation reduction reaction[16,17]. As a result, boosting photocatalytic activity requires improvements in the quantity of generated electron–hole pairs, separation efficiency, and carrier utilization efficiency.

Direct synthesis of MIL-125 using traditional hydrothermal/solvothermal procedures is still the most widely utilized approach[18]. Solvents have a vital role in the crystallinity of finished goods, and the ideal solvent combination is often discovered by trial-and-error. Another important aspect that influences the shape of MOFs formed is the concentration of reactants[19]. Herein, we present a simple and efficient scheme to fabricate catalytic MOF by a solvothermal process. Furthermore, this study presents a novel and highly efficient photocatalytic degradation of crude oil spill using MIL-125.

Materials and methods

Materials. Terephthalic acid (H_2BDC), HPLC methanol (MeOH), and anhydrous di-methyl formamide (DMF) were purchased from Fischer Scientific, UK. Titanium isopropoxide (TTIP) was produced in Sigma Aldrich, USA. Saline Water (TDS = 27,800 ppm) was taken directly from the Mediterranean Sea, Alexandria, and crude oil from the western desert, Egypt with the main characteristics shown in Table S1.

Methods. *Preparation of MIL-125.* The preparation method is shown in Fig. 1; in which 6.0 mmol of terephthalic acid (H_2BDC) was first dissolved into a mixed solvent of methanol (MeOH) and anhydrous dimethyl formamide (DMF) with a ratio 1:9. The solution was then treated with 1.9 mmol of titanium isopropoxide (TTIP) $Ti(OCH(CH_3)_2)_4$ for 1 h while stirring. The mixture was then sonicated for 25 min and transferred into a stainless-steel autoclave system (volume: 150 mL), reacting at 150 °C for different reaction times (18, 48) h[9,20–22]. To eliminate other unreacted organic species in the mixture, the yellow solid result was washed twice with a mixed solvent of (DMF and methanol). Afterward, the solid product was isolated by centrifugation. Finally, the white powder was acquired after vacuum drying it overnight in an oven at 80 °C[23]. The prepared MIL-125 samples were coded (MT18, MT48).

Characterization of the prepared MOFs. Fourier transform—infrared (FT-IR). The functional groups of MIL-125 samples were investigated using a Fourier transform—IR spectrophotometer (FTIR-8400S, Shimadzu) with a resolution of 2 cm^{-1}. The powder samples were tested in the (4000–350) cm^{-1} wavenumber range.

Scanning electron microscope (SEM). Scanning electron microscopy (SEM) (JEOL JSM 6360LA, Japan) was used to investigate the microstructure and surface morphology of all prepared samples (MT18, MT48). Before SEM imaging, the powders were sputter-coated with gold using a sputter-coating unit.

Raman analysis. A SENTERRA Raman Microscope with laser selectors (532, 633, and 785) nm was used to collect Raman spectra; the wavelength and power of the laser employed as an excitation source were 514.5 nm and 20 mW, respectively. The incident light was focused on the prepared samples and the radiation scattered by the sample was collected using a 50 objective (back-scattered configuration). A single spectrum required 360 s to acquire.

x-ray diffraction (XRD). X-ray diffraction scans of samples were obtained using (X-ray 7000 Shimadzu-Japan) at room temperature. The degree of crystallinity was determined by applying Bragg's low where 2θ is in the range of 5°–80°, with the X-ray source being a Cu target produced at 30 kV and 30 mA and a scan speed of 4° per minute. The crystallite size is determined from the broadening of corresponding X-ray spectral peaks by the Scherrer formula[24]:

$$D = K\lambda/(\beta\cos\theta)$$

$$\beta = [FWHM \times (\pi/180)]$$

where D is the crystallite size (dimension), λ is the wavelength of the X-ray radiation (Cu Kaα = 0.15418 nm), K is a constant (shape factor) usually taken as 0.89, θ is the angle between the incident and reflected rays and β is the line width at half-maximum height.

Thermogravimetric analysis (TGA). Thermogravimetric analysis is a sort of testing that is done on samples (5 mg) to assess weight loss variations as a result of temperature changes (using TGA-50 Shimadzu). This procedure was carried out at temperatures ranging from 50 to 800 °C, with a heating rate of 10 °C min^{-1} and a nitrogen flow rate of 20 ml min^{-1}. This technique is used to test the prepared MOFs' thermal stability.

Surface area Brunauer, Emmett and Teller (BET). The physical adsorption of an N_2 gas on the surface of the solid and the amount of adsorbate gas corresponding to a monomolecular layer on the surface are used to calculate the specific surface area of the prepared MOFs. Physical adsorption is caused by relatively modest interactions (van der Waals forces) between adsorbate gas molecules and the test samples' adsorbent surface area. A volumetric or continuous flow approach (Quantachrome Corporation Nova 1000, version 6.11 high speed, gas sorption analyzer) at 77 K can be used to determine the amount of gas adsorbed. Before the measurements, the samples were activated at 120 °C for 6 h[21,25].

Optical properties. The samples' optical characteristics were recorded to figure out where in the electromagnetic spectrum they absorb light. The UV–Vis spectrum of prepared MIL-125 was recorded using a UV–Vis spectrophotometer (T60 UV–visible) at wavelength scan ranges from 270 to 650 nm.

Photocatalytic degradation test. The prepared MOFs catalysts (MT18, MT48) were tested for the photocatalytic degradation of oil spills using mixed light sources (UV, and visible), and the experimental conditions are shown in Table S2. Each experiment was designed by adding (40 µL) crude oil to (100 mL) seawater under continuous stirring[26]. Firstly, the solution was kept in the dark for 30 min under continuous stirring then irradiation with UV–Vis light (a tungsten lamp of 100-W intensity as a source of visible light and four UV lamps of 2-W each as a source of UV light) was performed and the samples were taken each 30 min and then centrifuged to remove the catalysts. Samples were mixed with an equal volume of toluene with vigorous stirring for 30 min. Leave samples in a separating funnel then measure the remaining hydrocarbons in an aqueous layer by using UV-spectrophotometer at λ = 420 nm and calculate removal efficiency (RE%) using the following equation[27,28]

$$RE\% = \frac{[TH\ Control - TH\ treated]}{TH\ Control} \times 100$$

where *TH Control* is the oil concentration of the control and *TH Treated* is the oil concentration of the degraded sample.

All the photodegradation experiments were carried out in duplicate with the prepared photocatalyst. Gas Chromatography/Mass Spectrometry (GC/MS Shimazu QP2010 ultra) can help to make conclusive identification of compounds. These were the GC/MS operating conditions; the oven initial temperature was 80 °C for 0 min, raged at 10 °C min^{-1} to 240 °C, and then held for 2 min. The temperature was then ramped to 280 °C at 5 °C min^{-1}, and then held at 280 °C for 10 min. The injection temperature and volume were 250 °C and 1 µL, respectively. The split ratio was 20:1. The carrier gas used was He while the solvent delay time was 2.50 min. The transfer and source temperatures were 250 °C and 150 °C, respectively. Scanning was done from 50 to 500 Da and the column dimension was 27.0 m × 250 µm.

Results and discussion

The reaction of titanium isopropoxide as a metal precursor with terephthalic acid as an organic ligand in a proper percentage of solvent mixtures (*N*,*N*-dimethylformamide (DMF), and methanol) led to well-crystallized white powder of MIL-125. MIL-125 is composed of basic units of $Ti_8O_8(OH)_4$-$(O_2C$-C_6H_5-$CO_2)_6$ and is built up from cyclic octamers constructed from corner or edge-sharing octahedral titanium units, as shown in Fig. S1. These octamers are connected to 12 other cyclic octamers through H_2BDC linkers, leading to a porous three-dimensional quasi-cubic tetragonal structure having two types of cages, an octahedral (12.5 Å) and a tetrahedral (6 Å) cage, accessible through narrow triangular windows of ca. 6 Å[25].

IR and Raman spectra in Fig. 2A,B were used to analyze the structure and morphology of the prepared samples (MT18, MT48). All IR spectra show characteristic vibrational bands in the region of (1400–1700) cm^{-1} for the carboxylic acid functional group of the Ti-coordinated MOF structure. Two absorption bands around (1640, and 1500) cm^{-1} can be assigned to carbonyl asymmetric stretching vibrations, whereas the bands at (1571, and 1628) cm^{-1} could be ascribed to the phenyl C=C ring stretching and the C=O stretching[27]. The band at 1260 cm^{-1} belongs to the C–H symmetric stretching vibrations of the benzene ring, which is assumed by the Raman band at 1611 cm^{-1}[20]. The IR region of (400–800) cm^{-1} shows the Ti–O–Ti–O (Ti-oxo clusters) vibrations[20,21]. The bending and symmetric stretching of the framework Ti–O–Ti–O octatomic ring species may be seen at Raman bands (546, 1234, and 1414) cm^{-1}. The resonance-enhanced Raman band at 703 cm^{-1} is attributed to the framework titanium species in octahedral coordination settings, i.e., every single titanium atom is coupled to six oxygen atoms. The terephthalic acid ligand activates MT Raman, as evidenced by bands indexed at (1618, 1455, 1181,

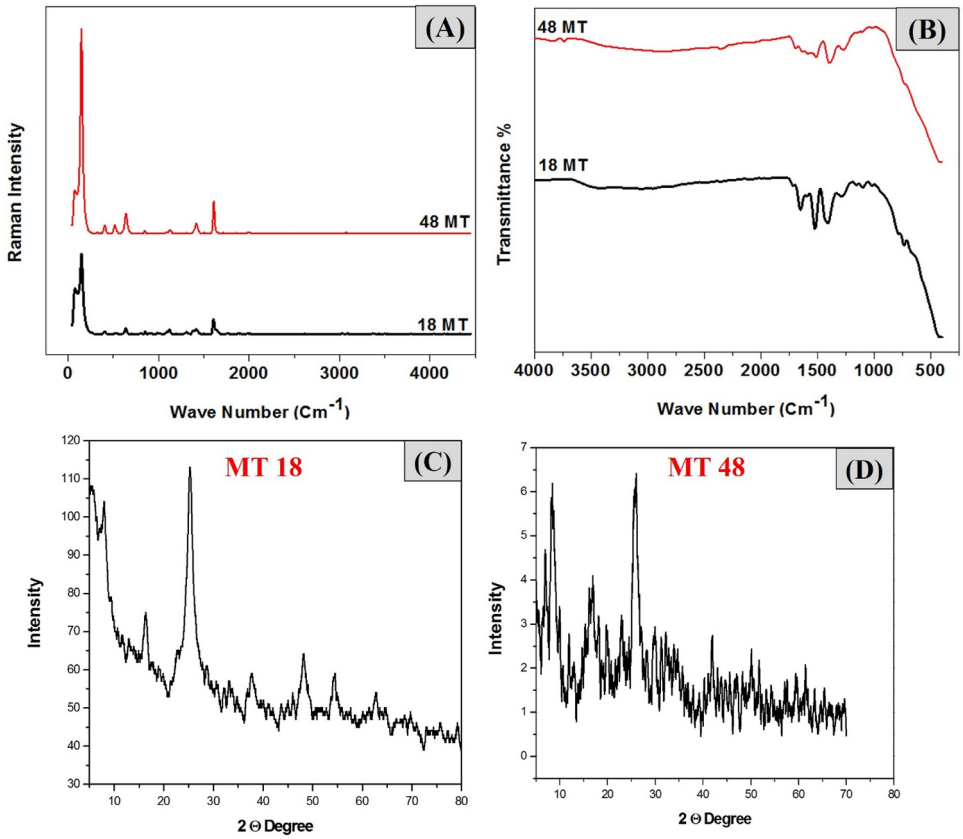

Figure 2. Characterization schemes of the prepared samples (**A**): Raman analysis, (**B**): FTIR analysis, (**C**,**D**): XRD of MT18, and MT48, respectively.

Samples	FWHM (degree)	2θ (degree)	D (crystal size) (nm)
MT18	1.15	25.19	7.3
MT48	1.14	26.27	7.0

Table 1. The crystal size calculation from XRD structure according to Debye Scherrer equation.

and 1138) cm^{-1}, which correspond to the in-plane vibrational modes of aromatic rings, and bands centered (865 and 641) cm^{-1}, which correspond to the vibrational modes of the aromatic rings' C–H and C=C bonds[29].

XRD displays in Fig. 2C,D, where the porous crystalline carboxylate-based MIL-125 is reported in 2009 by Serre et al., which were synthesized by direct solvothermal[30]. Fine powders of MIL-125 were acquired and their structure was determined by synchrotron powder XRD. The MIL-125 framework, Fig. S1, is composed of cyclic $Ti_8O_8(OH)_4(COO)_{12}$ octamers linked by terephthalic linkers to an edge-and-corner-sharing $TiO_5(OH)$ octahedron. The units are arranged in a centered cubic (cc) fashion, packing into the quasi-cubic tetragonal lattice, and each octamer has 12 units neighbors. The 3D structure has two types of cages corresponding to the octahedral and tetrahedral vacancies of cc packing, with effectively accessible diameters of 12.55 Å and 6.13 Å, respectively, and connected by triangular windows of 5–7 Å[18]. Because the photocatalytic activity is dependent on the active sites which are also influenced by the crystallite size, which is calculated using the Debye–Scherrer equation. It is found that the crystallite size of MT48 is 7 nm which is a little smaller than for MT18 as shown in Table 1.

The nitrogen adsorption–desorption isotherms, pore diameter, and pore volume of MIL-125 catalysts are shown in Fig. 3. Table 2 shows the pore size distribution displays pores with a diameter between (4.6 and 9.2) nm, for MT48 and MT18 respectively, which correspond to the microporous and mesoporous contributions, respectively, confirming the multimodal distribution. The MT48 catalyst's BET-specific surface area and total pore volume were 301 $m^2\ g^{-1}$ and 0.2444 $cm^3\ g^{-1}$ respectively, showing that it is a highly porous material. More active sites would be exposed if mesopores with a bigger surface area were formed, which would boost photocatalytic activity.

SEM images Fig. 4A,B reveal that both (MT18, MT48) samples are made up of particles with typical circular plate-like morphology[9] with particle sizes (258 ± 89, 234 ± 65) nm, respectively. The thermogravimetric analysis (TGA), in Fig. 4C, indicates a steady mass loss of the prepared MOFs before 800 °C. The first weight loss

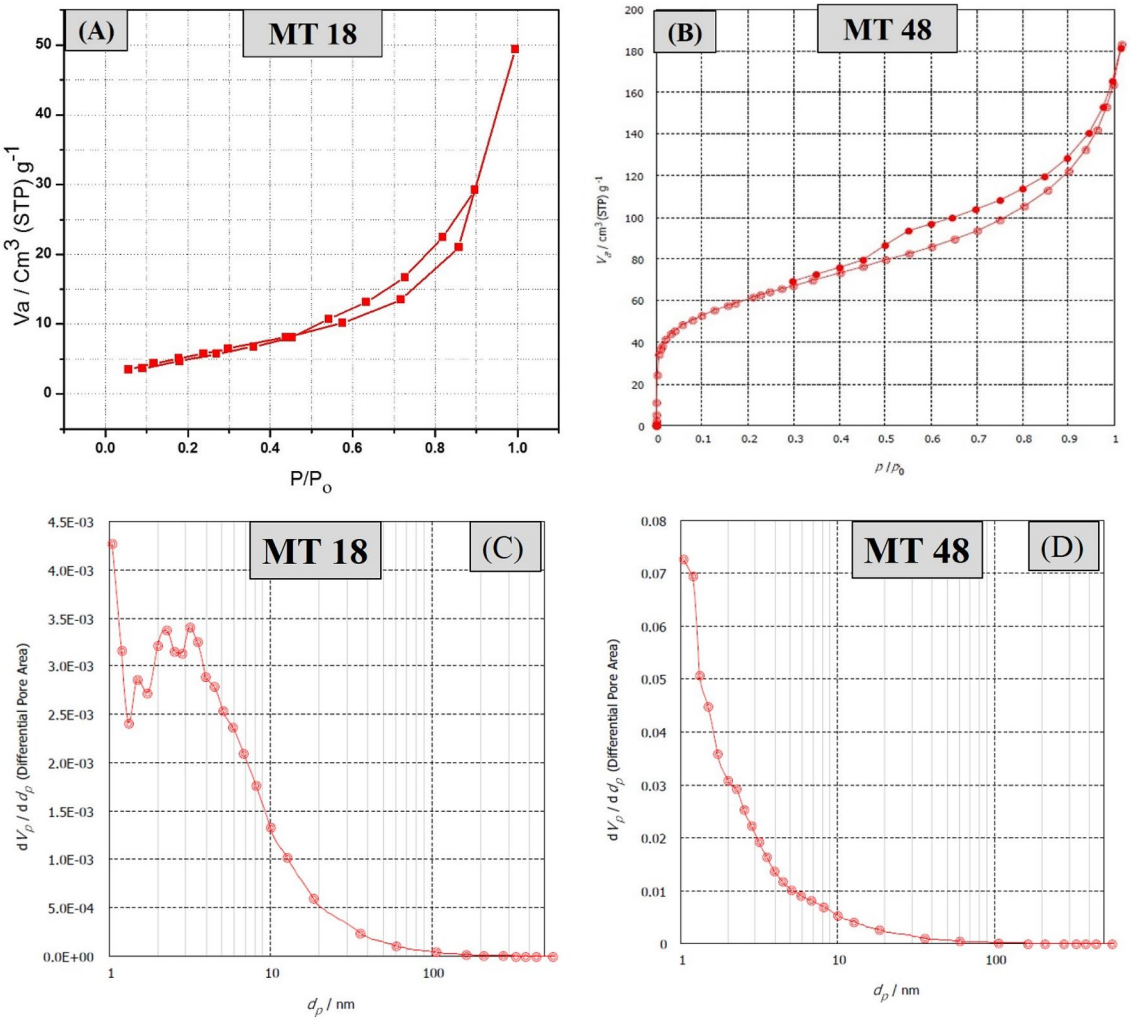

Figure 3. (**A**,**B**) Adsorption/desorption isotherm of both MT18, and MT48 samples, and (**C**,**D**) BJH-plot adsorption branch, adsorptive N2, adsorption temperature 77.350 K of both MT18, and MT48.

Samples	S_{BET} (sq. m g^{-1})	Total pore volume (V pore) (cm^3 g^{-1})	Average pore diameter (nm)
MT18	21.07	0.040083	9.2604
MT48	301.10	0.2444	4.6352

Table 2. Textural properties of MIL-125 catalysts.

before 200 °C at (80 °C, 61 °C) with weight loss (3.6%, 2.6%) for (MT18, MT48), respectively. This may be to the elimination of physically adsorbed gases, moisture, and DMF from the pores presumably owing to solvate evaporation[31]. The second weight loss between (200–500) °C is due to the framework disintegration[32], which eventually produces amorphous TiO_2 residue[33]. The residues were (75.33, and 49) % of the initial mass for both (MT18, and MT48), respectively.

Optical characterization. The optical properties of prepared MOFs (MT18, MT48) were investigated using the UV–VIS spectrum which is shown in Fig. 5A. Due to the octahedral coordination in titanium species, the two prepared samples (MT18, MT48) possess a broad absorption edge at wave length (310 nm), MT18, MT48 absorb only at wavelength below 310 nm, inducing excitation from HOMO, made of π states in the ligand and O(2p) in the metal-oxo cluster, into the LUMO defined by Ti(3d), leaving behind holes near the Ti-oxo cluster[9,34,35]. The optical bandgap (Eg) demonstrates a relationship between the absorption coefficient and the incident photon energy and can be calculated by using the following Tauc's equation[35,36].

$$\alpha h\nu = A\left(h\nu - Eg\right)\mathrm{n}$$

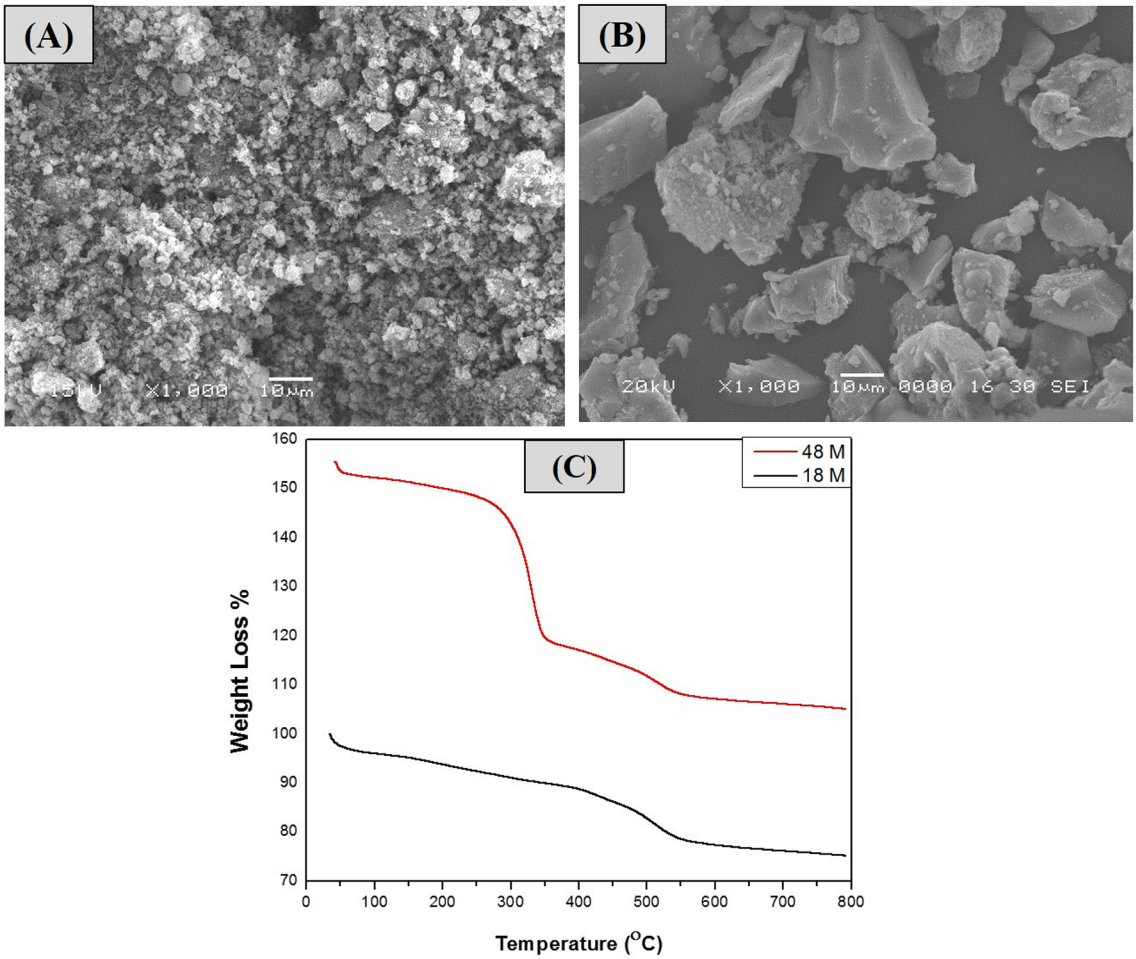

Figure 4. SEM images of (**A** MT18, **B** MT48), and (**C**) thermogravimetric analysis (TGA) of both MT18, MT48.

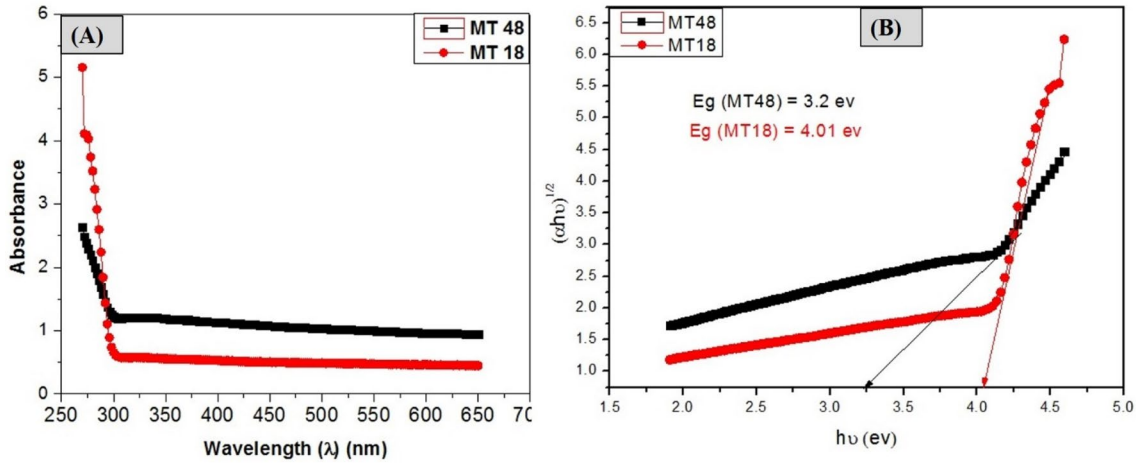

Figure 5. Optical behavior of MT18, MT48 (**A**) UV–Vis spectrum, (**B**) optical band gap plot.

$$h\nu = 1240/\lambda$$

where α is the coefficient of the absorption, hυ is the incident photon energy, A is a constant, Eg represents the bandgap, and n is determined based on the type of optical transition of prepared MOFs.

These materials have an indirect optical transition, thus n = 2. The optical energy gap (Eg) can be deduced from plotting the relationship between $(\alpha h\upsilon)^{1/2}$ and photon energy (hυ) for MT18 and MT48 as shown in Fig. 5B.

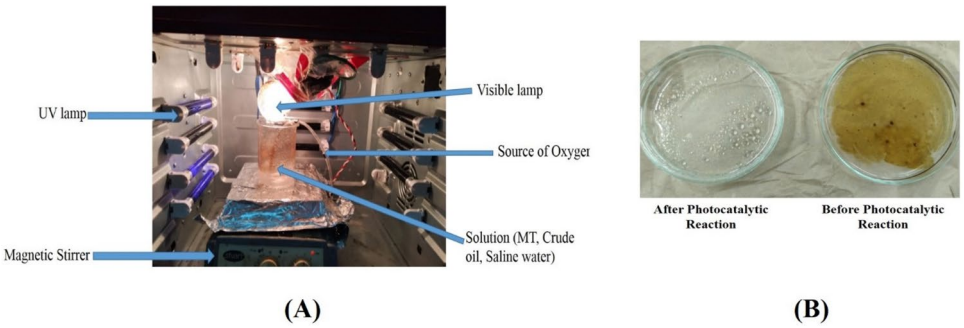

Figure 6. Photo-degradation study of (crude oil/saline water) samples by using different prepared MOF samples (18 MT, 48 MT).

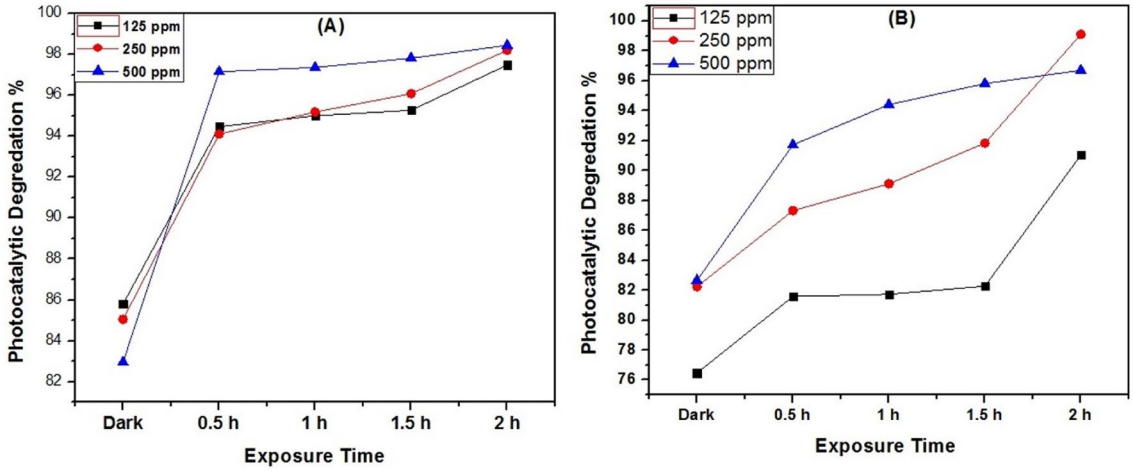

Figure 7. Photocatalytic degradation efficiency of crude oil, using different prepared samples (**A** MT18 and **B** MT48).

The calculated Eg of MT18 and MT48 is ~ 4.03 eV and ~ 3.2 eV, respectively, from the intercept of the tangent to the line. The reduction of band gap values from 4.03 eV for MT18 to 3.2 eV for MT48 may be due to the particle size decreasing from (258 to 234) nm as the solvothermal reaction time increase from (18 to 48) h[37].

Photocatalytic degradation of crude oil spills. Figure 6 shows the photo-degradation study of (crude oil/saline water) samples by using different MOF catalysts and it clearly shows that the disappearance of oil spills after photocatalytic reaction using MT18 and MT48. The concentration of crude oil before and after photodegradation can be determined using UV–Vis spectrophotometry and GC/MS technique. Figure 5 shows the UV–Vis spectrophotometry of degraded crude oil with respect to using the light as controlled value (absorbance = 3.344). Generally, the two prepared MIL-125 samples display a high efficiency toward the degradation of crude oil. Figure 7A shows that the use of different doses of MT18 as photocatalyst (125, 250, and 500) ppm in the degradation of crude oil spill revealed high degradation efficiencies reached 98.4% after 2 h of irradiation. On the other hand, Fig. 7B shows that using 250 ppm of MT48 as photocatalyst can degrade about 99% of crude oil spills after 2 h of irradiation. The MT48 has little more degradation efficiency under (UV–Vis light) this is due to the lower optical band gap (3.2 eV) and higher surface area (301.1 $m^2 g^{-1}$)[37]. The trend observed in the UV–Vis spectrophotometry analysis is agreed with the optical properties and morphological characterization results of prepared photocatalyst.

The GC/MS chromatograms of the analyzing wastewater samples before and after photodegradation are presented in Fig. 8. This analysis shows that water contaminated with crude oil spills (Control) contains different compounds such as Pentane-2-methyl, Tetrahydrofuran (THF), Cyclohexane, 6-Bromo-4-(2-choro-phenyl)-2-piperan, Benzene, (1-butylhexadecl), Benzene, (1-methylnonyl), Benzene, (1-buylheptyl), Benzene, (1-propyloctyl), Octadecane and Benzene, (1-pentylheptyl). The obtained chromatograms after photocatalytic degradation using MT18 and MT48 cleared that all mentioned compounds are degraded with high efficiencies and their concentrations become nil[38].

Kinetics of the reaction rate. Under various experimental conditions, our findings indicated that MIL-125 could be used to degrade marine oil spills. The photoreaction process can be divided into two stages based on the kinetic reaction curves in Fig. 9. First, the concentration decreased rapidly at the start of the irradiation,

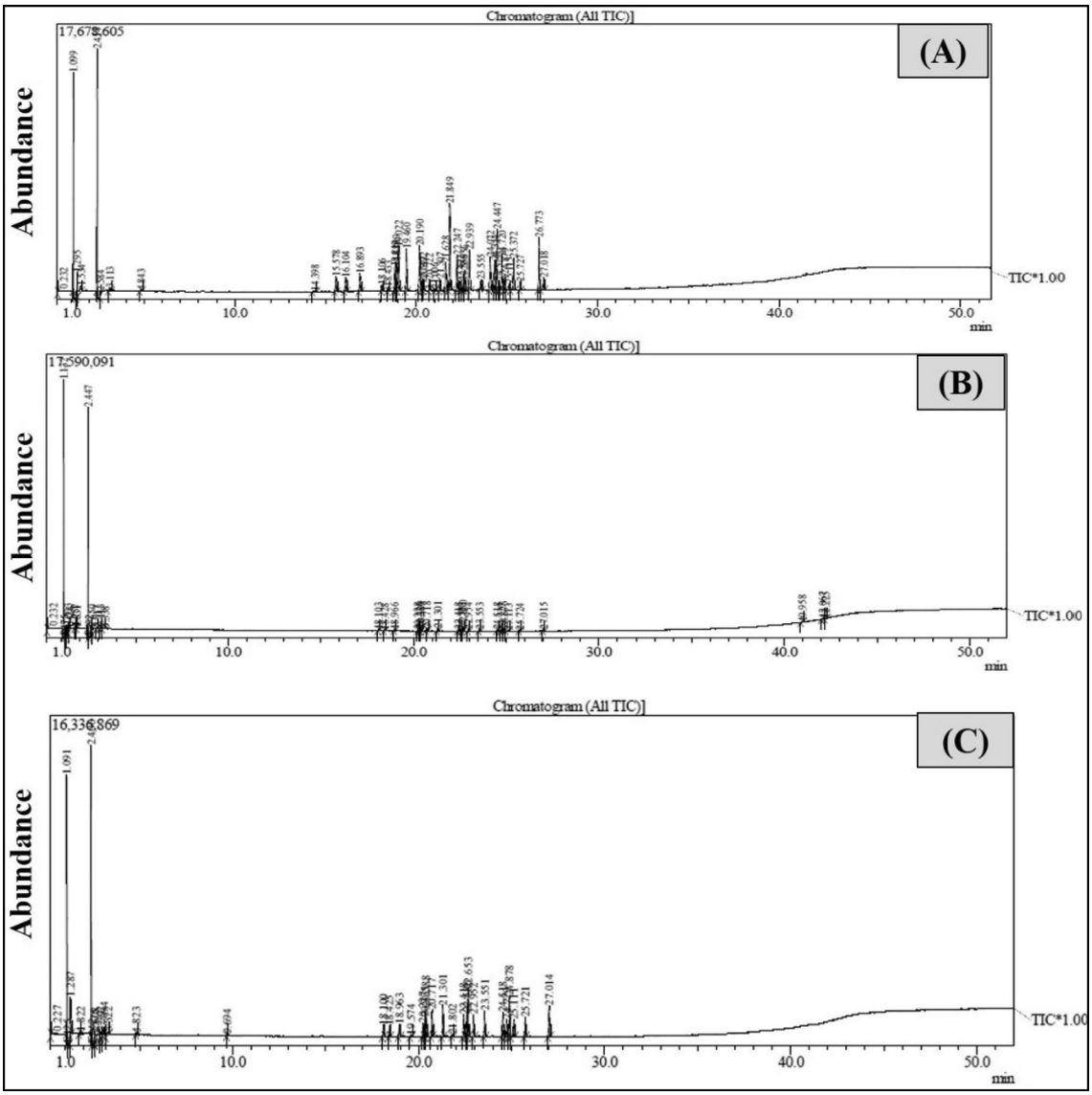

Figure 8. Chromatogram of crude oil photocatalytic degradation (**A** control, **B** degraded oil using MT18, and **C** degraded oil using MT48) after 2 h irradiation.

and the photoreaction confirmed a first-order kinetic pattern. Secondly, the concentration was nearly stabilized. According to the first-order kinetic reaction:

$$ln(Co/Ct) = kt$$

$$t1/2 = ln2/k$$

where C_o is the initial reaction concentration of oil; C_t is the concentration of oil measured at a fixed time; t is irradiation time, and K is is the reaction rate determined by the linear plot of In (C_o/C_t) versus the time. Table 3 summarizes the kinetic data from this study's photo-degradation of oil under various experimental conditions. According to our results, photochemical degradation is an effective method for removing petroleum hydrocarbons from seawater.

Conclusions

From this research, it is possible to conclude that, efficient MIL-125 photocatalysts have been successfully prepared via a facile solvothermal method. The sample prepared at 150 °C and a reaction time of 48 h (MT48) has a low crystal size of 7 nm and a particle size of 234 nm with an optical bandgap of 3.2 eV and a surface area of 301 $m^2 g^{-1}$. Based on GC/MS and UV/Vis photodegradation results, the two prepared samples show high efficiency toward the degradation of crude oil. And the use of 250 ppm of MT48 photocatalyst under UV–Vis irradiation can degrade about 99% of oil spills in water. This study presents a novel and highly efficient photocatalytic degradation of crude oil spills using MIL-125.

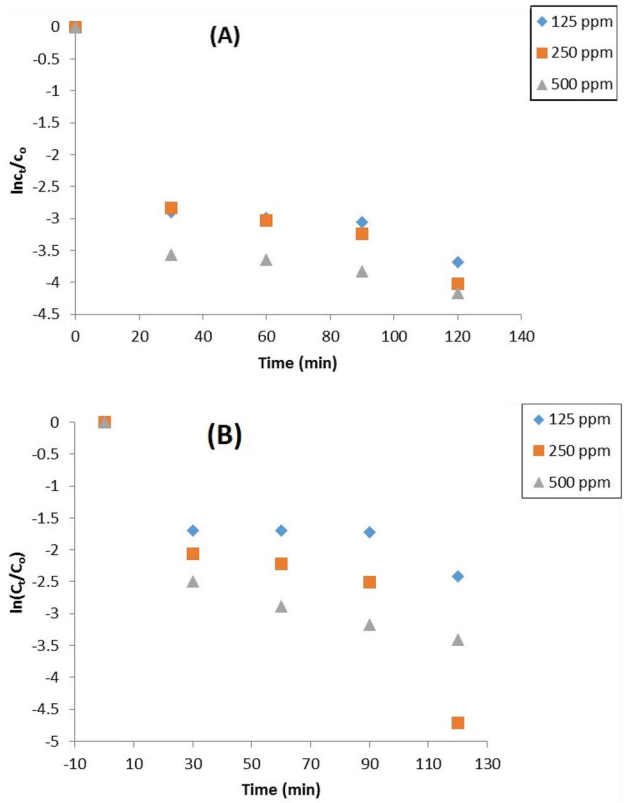

Figure 9. Kinetic study of photocatalytic degradation of oil spills using (**A**) MT18, (**B**) MT48.

Catalyst dose (ppm)		k (min^{-1})		$t_{1/2}$ (min)	
MT18	MT48	MT18	MT48	MT18	MT48
125	125	0.025	0.0162	4.382	4.816
250	250	0.028	0.0329	4.268	4.107
500	500	0.0286	0.025	4.247	4.382

Table 3. Kinetic data of photodegradation of oil spills using prepared MOFs under different conditions.

Data availability

The generated and analyzed data during the current study supplied in this manuscript and is readily available from the corresponding author upon reasonable request.

Received: 25 August 2022; Accepted: 13 December 2022
Published online: 23 December 2022

References

1. Zhang, B. *et al. Marine Oil Spills-Oil Pollution, Sources and Effects* 2nd edn. (Elsevier, 2018).
2. Luo, C. *et al.* Efficient biodegradation of phenanthrene using Pseudomonas stutzeri LSH-PAH1 with the addition of sophorolipids: Alleviation of biotoxicity and cometabolism studies. *Environ. Pollut.* **301**, 119011. https://doi.org/10.1016/j.envpol.2022.119011 (2022).
3. King, S. M. *et al.* Photolytic and photocatalytic degradation of surface oil from the Deepwater Horizon spill. *Chemosphere* **95**, 415–422. https://doi.org/10.1016/j.chemosphere.2013.09.060 (2014).
4. Shivaraju, H. P., Muzakkira, N. & Shahmoradi, B. Photocatalytic treatment of oil and grease spills in wastewater using coated N-doped TiO2 polyscales under sunlight as an alternative driving energy. *Int. J. Environ. Sci. Technol.* **13**, 2293–2302. https://doi.org/10.1007/s13762-016-1038-8 (2016).
5. Assi, H. *et al.* Titanium coordination compounds: From discrete metal complexes to metal-organic frameworks. *Chem. Soc. Rev.* **46**, 3431–3452. https://doi.org/10.1039/c7cs00001d (2017).
6. Chang, Y. J. *et al.* Ultrahigh efficient laser desorption ionization of saccharides by Ti-based metal-organic frameworks nanosheets. *Anal. Chim. Acta* **1032**, 91–98. https://doi.org/10.1016/j.aca.2018.06.035 (2018).
7. Hu, N. *et al.* Amino-functionalized titanium based metal-organic framework for photocatalytic hydrogen production. *Molecules* https://doi.org/10.3390/molecules27134241 (2022).

8. Li, L., Wang, X. S., Liu, T. F. & Ye, J. Titanium-based MOF materials: From crystal engineering to photocatalysis. *Small Methods* **4**, 1–28. https://doi.org/10.1002/smtd.202000486 (2020).
9. Wang, J. *et al.* Ti-based MOFs: New insights on the impact of ligand composition and hole scavengers on stability, charge separation and photocatalytic hydrogen evolution. *Appl. Catal. B Environ.* **283**, 119626. https://doi.org/10.1016/j.apcatb.2020.119626 (2021).
10. Wang, X. S., Li, L., Li, D. & Ye, J. Recent progress on exploring stable metal-organic frameworks for photocatalytic solar fuel production. *Sol. RRL* **4**, 1–34. https://doi.org/10.1002/solr.201900547 (2020).
11. Photocatalytic, F. M. Achievements and perspectives in metal—organic nitrogen reduction (2022).
12. Gao, J. *et al.* A p–type Ti(iv)–based metal–organic framework with visible–light photo–response. *Chem. Commun.* **50**, 3786–3788. https://doi.org/10.1039/c3cc49440c (2014).
13. Assi, H. *et al.* Investigating the case of titanium(IV) carboxyphenolate photoactive coordination polymers. *Inorg. Chem.* **55**, 7192–7199. https://doi.org/10.1021/acs.inorgchem.6b01060 (2016).
14. Dhakshinamoorthy, A., Asiri, A. M. & García, H. metal-organic framework (MOF) compounds: Photocatalysts for redox reactions and solar fuel production. *Angew. Chem. Int. Ed.* **55**, 5414–5445. https://doi.org/10.1002/anie.201505581 (2016).
15. Sun, D. & Li, Z. Robust Ti- and Zr-based metal-organic frameworks for photocatalysis. *Chin. J. Chem.* **35**, 135–147. https://doi.org/10.1002/cjoc.201600647 (2017).
16. Wang, C. C., Yi, X. H. & Wang, P. Powerful combination of MOFs and C_3N_4 for enhanced photocatalytic performance. *Appl. Catal. B Environ.* **247**, 24–48. https://doi.org/10.1016/j.apcatb.2019.01.091 (2019).
17. Fu, Y. *et al.* An amine-functionalized titanium metal-organic framework photocatalyst with visible-light-induced activity for CO_2 reduction. *Angew. Chem. Int. Ed.* **51**, 3364–3367. https://doi.org/10.1002/anie.201108357 (2012).
18. Zhu, J. *et al.* Titanium-based metal–organic frameworks for photocatalytic applications. *Coord. Chem. Rev.* **359**, 80–101. https://doi.org/10.1016/j.ccr.2017.12.013 (2018).
19. Chen, X. *et al.* Recent advances in titanium metal–organic frameworks and their derived materials: Features, fabrication, and photocatalytic applications. *Chem. Eng. J.* **395**, 125080. https://doi.org/10.1016/j.cej.2020.125080 (2020).
20. Hu, S. *et al.* Solvothermal synthesis of NH2-MIL-125(Ti) from circular plate to octahedron. *CrystEngComm* **16**, 9645–9650. https://doi.org/10.1039/c4ce01545b (2014).
21. Wen, G. & Guo, Z. G. Facile modification of NH2-MIL-125(Ti) to enhance water stability for efficient adsorptive removal of crystal violet from aqueous solution. *Colloids Surf. A Physicochem. Eng. Asp.* **541**, 58–67. https://doi.org/10.1016/j.colsurfa.2018.01.011 (2018).
22. Wang, S. *et al.* Toward a rational design of titanium metal-organic frameworks. *Matter* **2**, 440–450. https://doi.org/10.1016/j.matt.2019.11.002 (2020).
23. Kaur, M., Mehta, S. K. & Kansal, S. K. Amine-functionalized titanium metal-organic framework (NH2-MIL-125(Ti)): A novel fluorescent sensor for the highly selective sensing of copper ions. *Mater. Chem. Phys.* **254**, 123539. https://doi.org/10.1016/j.matchemphys.2020.123539 (2020).
24. Drits, V., Środoń, J. & Eberl, D. D. XRD measurement of mean crystallite thickness of illite and illite/smectite: Reappraisal of the Kubler index and the Scherrer equation. *Clays Clay Miner.* **45**, 461–475. https://doi.org/10.1346/CCMN.1997.0450315 (1997).
25. Kim, S. N. *et al.* Adsorption/catalytic properties of MIL-125 and NH2-MIL-125. *Catal Today* **204**, 85–93. https://doi.org/10.1016/j.cattod.2012.08.014 (2013).
26. Li, Y., Zhang, Q., Jiang, J. & Li, L. Long-acting photocatalytic degradation of crude oil in seawater via combination of TiO_2 and N-doped TiO_2/reduced graphene oxide. *Environ. Technol.* https://doi.org/10.1080/09593330.2019.1647291 (2019).
27. Zhang, S. *et al.* Defect-rich and electron-rich mesoporous Ti-MOFs based NH2-MIL-125(Ti)@ZnIn2S4/CdS hierarchical tandem heterojunctions with improved charge separation and enhanced solar-driven photocatalytic performance. *Appl. Catal. B Environ.* **262**, 118202. https://doi.org/10.1016/j.apcatb.2019.118202 (2020).
28. El-Borai, A. M., Eltayeb, K. M., Mostafa, A. R. & El-Assar, S. A. Biodegradation of industrial oil-polluted wastewater in Egypt by bacterial consortium immobilized in different types of carriers. *Pol. J. Environ. Stud.* **25**, 1901–1909. https://doi.org/10.15244/pjoes/62301 (2016).
29. Hlophe, P. V. & Dlamini, L. N. Synthesis of a semi-conductor-like MOF with black phosphorous as a composite for visible light-driven photocatalysis. *RSC Adv.* **9**, 37321–37330. https://doi.org/10.1039/c9ra08296d (2019).
30. Meenakshi, D.-H. *et al.* A new photoactive crystalline highly porous titanium(IV) dicarboxylate. *J. Am. Chem. Soc.* **131**, 25 (2009).
31. Chao, M. Y., Zhang, W. H. & Lang, J. P. Co2 and Co3 mixed cluster secondary building unit approach toward a three-dimensional metal-organic framework with permanent porosity. *Molecules* https://doi.org/10.3390/molecules23040755 (2018).
32. Peng, M. M. *et al.* Oxidation of ethylbenzene using nickel oxide supported metal organic framework catalyst. *Bull. Korean Chem. Soc.* **35**, 3213–3218. https://doi.org/10.5012/bkcs.2014.35.11.3213 (2014).
33. Hu, S. *et al.* Surfactant-assisted synthesis of hierarchical NH2-MIL-125 for the removal of organic dyes. *RSC Adv.* **7**, 581–587. https://doi.org/10.1039/c6ra25745c (2017).
34. Sun, D., Ye, L. & Li, Z. Visible-light-assisted aerobic photocatalytic oxidation of amines to imines over NH2-MIL-125(Ti). *Appl. Catal. B Environ.* **164**, 428–432. https://doi.org/10.1016/j.apcatb.2014.09.054 (2015).
35. Capano, G. *et al.* On the electronic and optical properties of metal-organic frameworks: Case study of MIL-125 and MIL-125-NH2. *J. Phys. Chem. C* **124**, 4065–4072. https://doi.org/10.1021/acs.jpcc.9b09453 (2020).
36. Mostafa, M., El Nady, J., Ebrahim, S. M. & Elshaer, A. M. Synthesis, structural, and optical properties of Mn^{2+} doped ZnS quantum dots for biosensor application. *Opt. Mater. (Amst.)* **112**, 110732. https://doi.org/10.1016/j.optmat.2020.110732 (2021).
37. Ghosh, R. *et al.* The effect of cluster size on the optical band gap energy of Zn-based metal-organic frameworks. *Dalt. Trans.* **44**, 13464–13468. https://doi.org/10.1039/c5dt02132d (2015).
38. Agyei-tuffour, B., Gbogbo, S., Dodoo-arhin, D., *et al* (2020) Photocatalytic degradation of fractionated crude oil: Potential application in oil spill remediation Photocatalytic degradation of fractionated crude oil: Potential application in oil spill remediation. https://doi.org/10.1080/23311916.2020.1744944.

Author contributions

Conceptualization, writing, methodology, validation, formal analysis, and data curation, M.S.S.; writing, review and editing, A.M.A.E.-A., R.R. All authors have read and agreed to the published version of the manuscript.

Funding

Open access funding provided by The Science, Technology & Innovation Funding Authority (STDF) in cooperation with The Egyptian Knowledge Bank (EKB).

Competing interests

The authors declare no competing interests.

Additional information

Supplementary Information The online version contains supplementary material available at https://doi.org/10.1038/s41598-022-26295-8.

Correspondence and requests for materials should be addressed to M.S.S.

Reprints and permissions information is available at www.nature.com/reprints.

Publisher's note Springer Nature remains neutral with regard to jurisdictional claims in published maps and institutional affiliations.